Human Molecular Genetics, 2014, Vol. 23, No. 10 **2665–2677**
doi:10.1093/hmg/ddt661
Advance Access published on December 30, 2013

Functional validation of a human *CAPN5* exome variant by lentiviral transduction into mouse retina

Katherine J. Wert[1,2,3], Jessica M. Skeie[4,5], Alexander G. Bassuk[4,6], Alicia K. Olivier[7], Stephen H. Tsang[1,2,4] and Vinit B. Mahajan[4,5,*]

[1]Bernard and Shirlee Brown Glaucoma Laboratory, Department of Pathology and Cell Biology, College of Physicians and Surgeons, [2]Edward S. Harkness Eye Institute and [3]Institute of Human Nutrition, College of Physicians and Surgeons, Columbia University, New York, NY 10032, USA [4]Omics Laboratory, [5]Department of Ophthalmology and Visual Sciences, [6]Department of Pediatrics and Neurology, [7]Department of Pathology, University of Iowa, Iowa City, IA, USA

Received October 7, 2013; Revised December 10, 2013; Accepted December 23, 2013

Exome sequencing indicated that the gene encoding the calpain-5 protease, *CAPN5*, is the likely cause of retinal degeneration and autoimmune uveitis in human patients with autosomal dominant neovascular inflammatory vitreoretinopathy (ADNIV, OMIM #193235). To explore the mechanism of ADNIV, a human *CAPN5* disease allele was expressed in mouse retinas with a lentiviral vector created to express either the wild-type human (*h*) *CAPN5* or the ADNIV mutant *hCAPN5-R243L* allele under a rhodopsin promoter with tandem green fluorescent protein (GFP) expression. Vectors were injected into the subretinal space of perinatal mice. Mouse phenotypes were analyzed using electroretinography, histology and inflammatory gene expression profiling. Mouse calpain-5 showed high homology to its human ortholog with >98% sequence identity that includes the ADNIV mutant residue. Calpain-5 protein was expressed in the inner and outer segments of the photoreceptors and in the outer plexiform layer. Expression of the *hCAPN5-R243L* allele caused loss of the electroretinogram *b*-wave, photoreceptor degeneration and induction of immune cell infiltration and inflammatory genes in the retina, recapitulating major features of the ADNIV phenotype. Intraocular neovascularization and fibrosis were not observed during the study period. Our study shows that expression of the *hCAPN5-R243L* disease allele elicits an ADNIV-like disease in mice. It further suggests that ADNIV is due to *CAPN5* gain-of-function rather than haploinsufficiency, and retinal expression may be sufficient to generate an autoimmune response. Genetic models of ADNIV in the mouse can be used to explore protease mechanisms in retinal degeneration and inflammation as well as preclinical therapeutic testing.

INTRODUCTION

Autosomal dominant neovascular inflammatory vitreoretinopathy (ADNIV, OMIM 193235) is a heritable autoinflammatory disease of the eye without systemic features. It is among the few Mendelian diseases with signs of autoimmunity and provides a key model for the study of neurodegeneration and neuroinflammation. ADNIV is unusual because it shows pathological features of several eye diseases that normally do not occur together. These include autoimmune uveitis, retinitis pigmentosa, proliferative diabetic retinopathy and proliferative vitreoretinopathy (1–4). ADNIV patients progressively lose vision caused by chronic intraocular inflammation, photoreceptor degeneration, retinal neovascularization, vitreous hemorrhage and intraocular fibrosis. These features occur in five stages over several decades until eyes become blind and phthisical (4).

Exome sequencing showed that ADNIV is likely caused by mutations in the catalytic domain of *CAPN5* (NP_004046) (4). Two different DNA mutations in *CAPN5* were discovered in two unrelated ADNIV families: c.728G>T, p.Arg243Leu and c.731T>C, p.Leu244Pro (4). The physiologic role of calpain-5 in the human or the mouse eye is not known. *CAPN5* encodes calpain-5, an intracellular calcium-activated cysteine protease. *Tra-3* is the calpain-5 ortholog in *Caenorhabditis elegans (C. elegans)* and is involved in neuronal degeneration and sex determination (5). The functions of some human calpains have been

*To whom correspondence should be addressed at: Department of Ophthalmology and Visual Sciences, the University of Iowa, 200 Hawkins Drive, Iowa City, IA 52242, USA. Tel: +1 3194675151; Fax: +1 3193560363; Email: mahajanlab@gmail.com

© *The Author 2013. Published by Oxford University Press. All rights reserved.*
For Permissions, please email: journals.permissions@oup.com

determined, and these play a role in several human diseases. Mutations in *CAPN3* cause limb-muscle girdle dystrophy type 2A. Single-nucleotide polymorphisms in calpain-10 are associated with type II diabetes mellitus (6). Excess calpain activity is associated with Alzheimer's disease (calpain 1) and myocardial infarction (calpains 1, 2 and 4).

Calpains target intracellular proteins through specific, limited proteolysis that often leads to target protein activation and regulation rather than degradation (7). For example, calpain-1 induces the translocation of apoptosis-inducing factor (AIF) from mitochondria to the nucleus after proteolytic cleavage (8). Calpain activity is tightly regulated by endogenous inhibitors and subcellular localization. The targets of calpain-5 are not known, but mutations in *CAPN5* could alter its proteolytic activity or specificity and effect downstream signaling pathways. It is possible that the alterations in distinct signaling cascades by mutant *CAPN5* could account for the various inflammatory, degenerative, vascular and fibrotic phenotypes observed in ADNIV patients. This hypothesis is supported by our clinical studies, in which intraocular steroids suppress inflammatory cell recruitment and angiogenic pathways, but not fibrotic or retinal degenerative pathways (9,10).

Next-generation exome sequencing is rapidly identifying candidate disease alleles in unexpected human genes, but the ability to functionally validate these candidate genes has not kept pace with the identification. Transient gene transduction may represent a more rapid and cost-efficient *in vivo* method in testing potential disease alleles in comparison with the development of transgenic mice. *CAPN5* is widely expressed, but the disease is restricted to the eye. A key therapeutic question is whether disease allele expression in the eye is sufficient to cause disease. In this case, ADNIV patients could be candidates for retinal gene therapy. Alternatively, if disease allele expression in the eye is not sufficient, therapies directed to cells outside the eye, such as calpain-5 expressing T cells, might be required. In this study, our goal was to test an ADNIV-causing allele in a mouse pre-clinical model. We engineered lentiviral vectors to express either the normal human (*h*) *CAPN5* or the ADNIV mutant *hCAPN5-R243L* gene in rod photoreceptor cells. Subretinal injections of the viral vectors into the perinatal mouse eye were used to determine whether the single c.728G>T nucleotide change would lead to an early and/or late-stage ADNIV-like phenotype. The successful creation of a pre-clinical model for ADNIV could be used to study the mechanisms of ADNIV disease progression, therapeutic interventions and other vitreoretinal diseases with similar phenotypes to ADNIV, such as uveitis or retinitis pigmentosa.

RESULTS

ADNIV Clinical Case

A 39-year-old female was first diagnosed with ADNIV at age 23 when she noticed blurred vision. Her visual acuity was 20/50 in both eyes. She showed features of the early, stage II form of ADNIV, characterized by 1+ vitreous cells, but no disc or retinal neovascularization (Fig. 1A). Goldmann visual field testing showed constriction of the I2e, I4e and V4e isopters OU (Fig. 1B). Electroretinography (ERG) recordings displayed a loss of photoreceptor cell responses (Fig. 1C). Dark-adapted

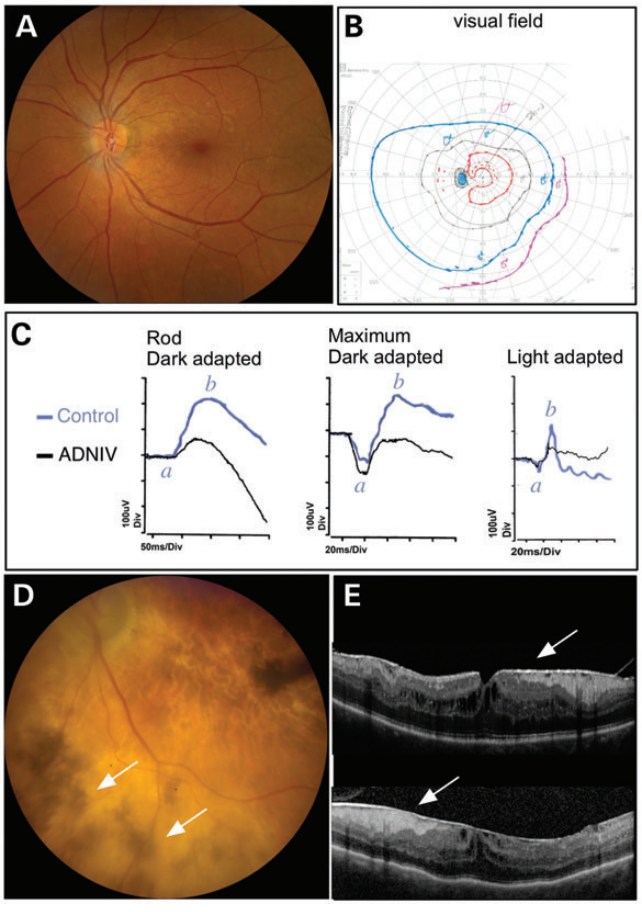

Figure 1. ADNIV Clinical Case. (**A**) The fundus image shows a normal vasculature, optic nerve and very little pigmentary change in the left retina in an early stage I–II case of ADNIV. (**B**) The visual field, however, reveals constriction of all isopters, which indicates reduced retinal light sensitivity to various intensities of light. (**C**) This was confirmed by electroretinography. Loss of maximal *b*-wave amplitudes (*b*) for the ADNIV human patient (black) compared with a normal control (blue) indicates a signaling defect in both rod and cone visual function. No significant change in the *a*-wave amplitudes (*a*) were noted between the ADNIV patient (black) and the control (blue) (**D**) Over two decades, stage III–IV disease develops. The retina shows signs of degeneration with extensive pigmentary changes (arrows) and atrophic changes throughout the fundus. The optic nerve becomes pale and the retinal vessels are attenuated. (**E**) Later, optical coherence tomography reveals fibrotic membranes, cystoid macular edema and distortion of the retinal layers.

0.01 rod response showed that maximal *b*-wave amplitudes (black) were ~65% of a normal human ERG response (blue). Dark-adapted 3.0 maximal combined ERG showed a modest reduction in *b*-wave amplitude (black), but with relatively normal amplitude of the *a*-wave. Interestingly, cone cells displayed borderline low amplitudes in the photopic ERG response (black) compared with a normal photopic ERG response (blue).

Over the next two decades, she showed signs of late ADNIV like her mother. Her cataracts were replaced with artificial intraocular lenses at age 29, and she was treated unsuccessfully with various immunosuppressive medications. Chronic inflammation was eventually controlled by surgical implantation of fluocinolone acetonide devices at age 36, and retinal neovascularization or neovascular glaucoma never developed (9). Nevertheless, her vision progressively deteriorated to

20/500, presumably owing to photoreceptor degeneration and intraocular fibrosis characteristic of stage III disease. Fundus examination revealed the development of patchy pigmentation and atrophy in the peripheral retina that had progressed to the center (Fig. 1D; arrows). Additionally, optical coherence tomography (OCT) detected cystoid macular edema (CME) and epiretinal membranes OU (Fig. 1E). With progression to stage IV disease, the reduction in maximal *b*-wave amplitudes is expected to continue to a complete loss of ERG response as occurred in her affected family members (4,11). Both she and her mother carried the c.728G>T, p.Arg243Leu mutation in the *CAPN5* gene. Immunosuppressive therapies for ADNIV are inadequate, there is no therapy for retinal degeneration and there are no specific therapies for calpains. To better understand and treat the early and late stages of ADNIV, a non-human model is needed.

Capn5 gene and transcript analysis

We considered development of a mouse model for ADNIV. Interrogation of genomic databases identified three possible mouse (*m*) *Capn5* transcripts on chromosome 7 and three corresponding (*h*) *CAPN5* transcripts on chromosome 11. Previous RNA-seq of human retina detected only a single *CAPN5* transcript (4). RNA-seq of a mouse retina was performed and also detected a single *Capn5* transcript (Fig. 2A and B). ADNIV mutations (red boxes) occur in exon 6, which codes for the catalytic (II) domain of calpain-5. This domain contains the three catalytic residues and calcium-binding sites (Fig. 2C; blue and orange boxes, respectively). Alignment of the primary amino acid sequence of *mCapn5* to its human ortholog showed 98% identity, including the amino acid mutated in the *hCAPN5* disease allele (R243L) (Fig. 2D; red boxes).

Calpain-5 is located in mouse photoreceptor cells

We previously reported that expression of calpain-5 was restricted to the inner and outer segments (IS and OS, respectively) of the rod and cone photoreceptors in the human retina (4). A similar expression pattern was observed in the mouse retina, where calpain-5 was present in the IS and OS of the photoreceptor cells (Fig. 3A and B). Interestingly, the mouse antibody also identified calpain-5 expression in the outer plexiform layer (OPL) close to the photoreceptor nuclei (Fig. 3C; arrow). Human retina was re-probed with a different anti-calpain-5 antibody (Abcam, Cambridge, MA), and immunofluorescence in the OPL was also detected (Fig. 3D; arrows).

Human *CAPN5* lentiviral vectors survive long term within the eye after subretinal injection

As *mCapn5* shared a nearly identical sequence and expression pattern with its human ortholog (Fig. 2), lentiviruses were constructed to express *hCAPN5* within the mouse retina. The lentivirus vector contained a rhodopsin promoter and a tandemly expressed green fluorescent protein (GFP) marker (Fig. 4A). There was no toxicity in cultured cells with the vectors, and our laboratory has performed subretinal injections of lentiviral vectors into the murine eye with no adverse side effects [data not shown; (12,13)]. Lentiviral constructs were designed with either wild-type *hCAPN5* or the ADNIV mutant *hCAPN5-R243L*. As calpains can escape regulatory control by overexpression (14–17), the wild-type *hCAPN5* was designed to test the effect of overexpression. The mutant *hCAPN5* was designed to test pathogenic effects of the patient-specific allele. A third construct without an insert was used to determine the nonspecific effect of GFP alone. Saline (no vector) injections were performed in control mice to control for the injection effect. The virus was injected into the subretinal space of the right eye on post-natal day (P) 5. The uninjected left eye also served as a matched control. Using autofluorescence (AF) live-imaging, punctate GFP expression was detected in ~20% of retinal cells from P5 through P180, indicating that the virus survived within the host without rejection (Fig. 4C). No GFP fluorescence was detected in the uninjected eyes (Fig. 4B).

hCAPN5-R243L reduces visual function in the mouse

In the early stages of ADNIV, patients show loss of the *b*-wave electroretinography (ERG) before signs of photoreceptor degeneration. To ascertain whether this phenotype could be detected in mice, serial ERGs were performed following subretinal injection of the lentiviruses. A reproducible ERG phenotype was observed at 3 months. Representative traces of dark-adapted 3.0 maximal combined ERG visual responses showed that, compared with the uninjected eye (blue), the *hCAPN5* lentiviral-injected eyes only showed a decrease in maximal *a*-wave amplitude, with no change in the *b*-wave (Fig. 5A; green). There was a greater loss of visual function within the *hCAPN5-R243L* lentiviral-injected eyes for both the *a*- and *b*-wave amplitudes (Fig. 5A; red), suggesting the disease allele had a greater detrimental effect.

We further examined the specific function of the rod and cone photoreceptor cells. Representative traces for the scotopic dim-light, rod-specific visual function displayed similar results to that of the dark-adapted maximal combined ERG visual response. A loss of the rod-specific *b*-wave amplitude was apparent in the eyes injected with the *hCAPN5* lentivirus (green) compared with the uninjected control eyes (blue), but there was again a greater loss of the rod *b*-wave amplitude in the *hCAPN5-R243L* lentiviral-injected eyes (Fig. 5B; red). The photopic ERG response was generated to examine the visual function of the cone cells, which were also affected in human ADNIV patients (Fig. 1G). Here, the *hCAPN5*-injected eyes appeared similar to controls (green and blue, respectively). However, there was a specific loss of the photopic *b*-wave amplitude in the *hCAPN5-R243L* lentiviral-injected eyes (Fig. 5C; red), as seen in the human ADNIV patient ERG (Fig. 1G). Although it was not previously reported, electrophysiological testing of the photopic *b*-wave may be an earlier, more sensitive test in humans. Overall, the representative ERG traces displayed a greater loss of visual function when the single amino acid change R243L was present in *hCAPN5*, and this R243L mutation may be a potential disease-causing allele in the mouse model of human ADNIV.

We next quantified the maximal amplitudes of each ERG result by comparing the ERG results for the *hCAPN5* (green) and *hCAPN5-R243L* (red) lentiviral-injected eyes, along with the two different control injections: saline or a lentivirus containing the rhodopsin promoter and GFP without the *hCAPN5* transgene inserted (blue). We then measured the *b*-wave amplitude differences by subtracting the untreated eye from the eye that

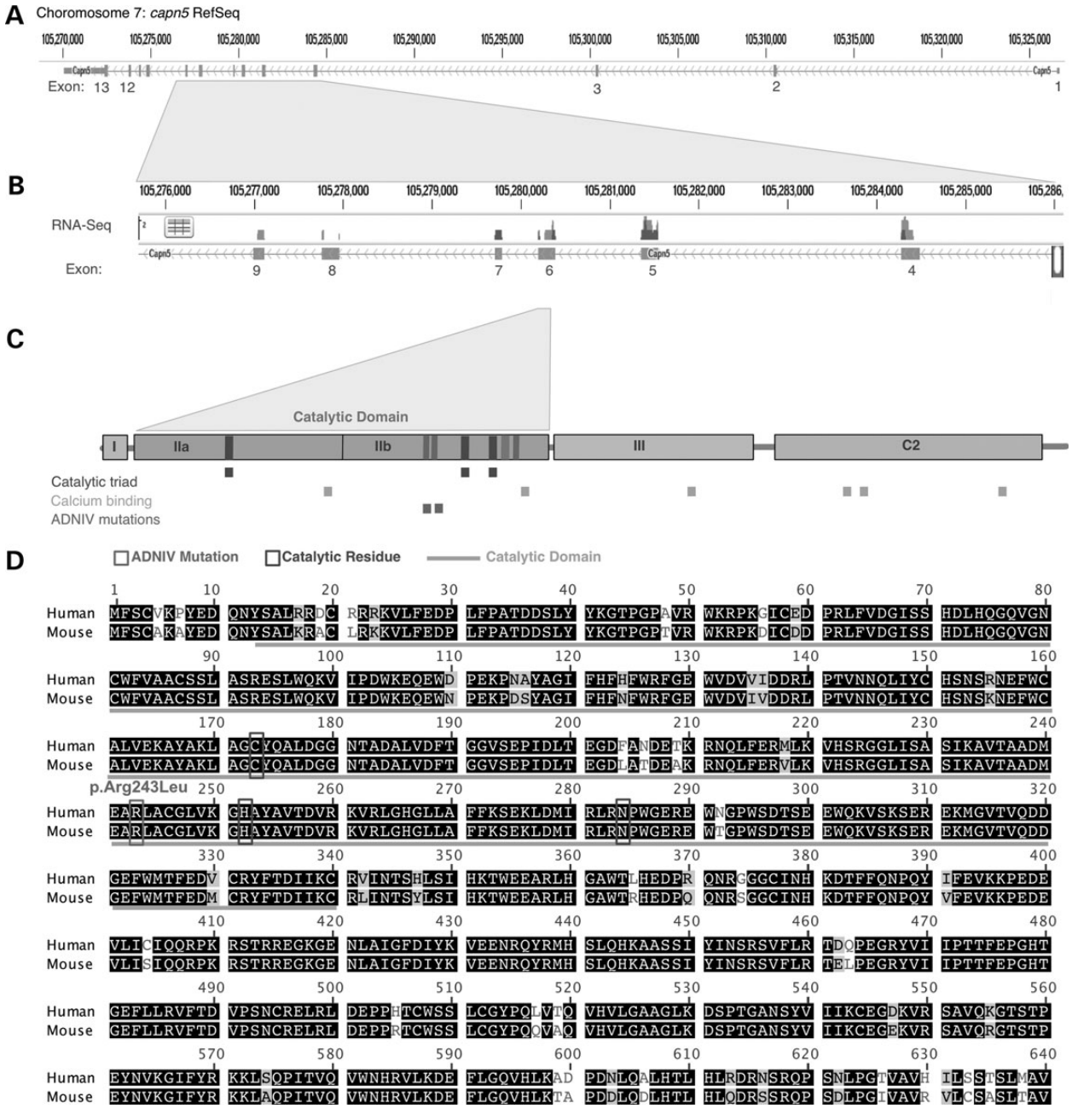

Figure 2. The mouse calpain-5 protein is highly homologous to its human ortholog. (**A**) Diagram of mouse *Capn5* exonic structure. (**B**) Representative RNA-Seq from mouse retina. Vertical bars above the corresponding exon represent reads from massive parallel sequencing of mouse retina. Note that exon 6 is the ortholog to the human exon for which *CAPN5* mutations have been identified in ADNIV patients. (**C**) Domain map shows the catalytic domain is encoded by exon 6. ADNIV mutations occur near the catalytic residues. (**D**) Protein alignment between calpain-5 in mouse and human species shows high conservation, including the site of R243L mutation.

received the injection, as shown in the cartoon diagram (Fig. 5D). This represented the difference of the subretinally-injected eye to its uninjected fellow eye for each ERG setting and allowed us to also compare the ERG results of each injected vector.

The dark-adapted 3.0 maximal combined ERG visual responses displayed expected background variation for the two control groups (blue) with no alteration in visual function (Fig. 5E). However, there was a loss of *b*-wave amplitudes in the eyes injected with the wild-type *hCAPN5* (green) and mutant *hCAPN5-R243L* (red) lentiviruses compared with their uninjected fellow eyes (96.2 $\pm$ 22.6 μV and 104.4 $\pm$ 16.7 μV, respectively; Fig. 5E). There was a significant difference between the *hCAPN5* visual responses in comparison with the GFP lentiviral-injected eyes; however, there was no significant difference between the *hCAPN5* lentiviral-injected eyes and the saline control injections. In contrast, there was a greater statistically significant loss of visual function in the *hCAPN5-R243L* lentiviral-injected eyes compared with both of the control

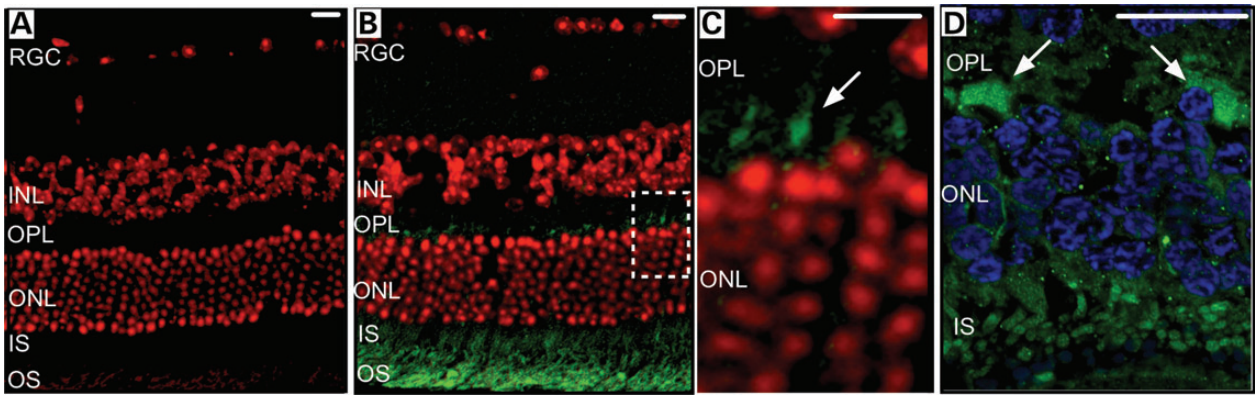

Figure 3. Calpain-5 is located in the mouse and human retina. (**A**) Retinal section of a wild-type C57BL/6J (B6) control mouse. (**B**) Retinal section of a wild-type B6 control mouse with CAPN5 protein located in the outer and inner segments of the photoreceptor cells. (**C**) Magnified view of the white-dashed box in B, showing calpain-5 localization in the outer plexiform layer (arrow). (**D**) Calpain-5 localization in the human retina outer plexiform layer (arrows). Red or blue, DAPI; green, mCAPN5 or hCAPN5. RGC, retinal ganglion cells; INL, inner nuclear layer; OPL, outer plexiform layer; ONL, outer nuclear layer; IS, photoreceptor inner segments; OS, photoreceptor outer segments. Scale bar = 20 μm.

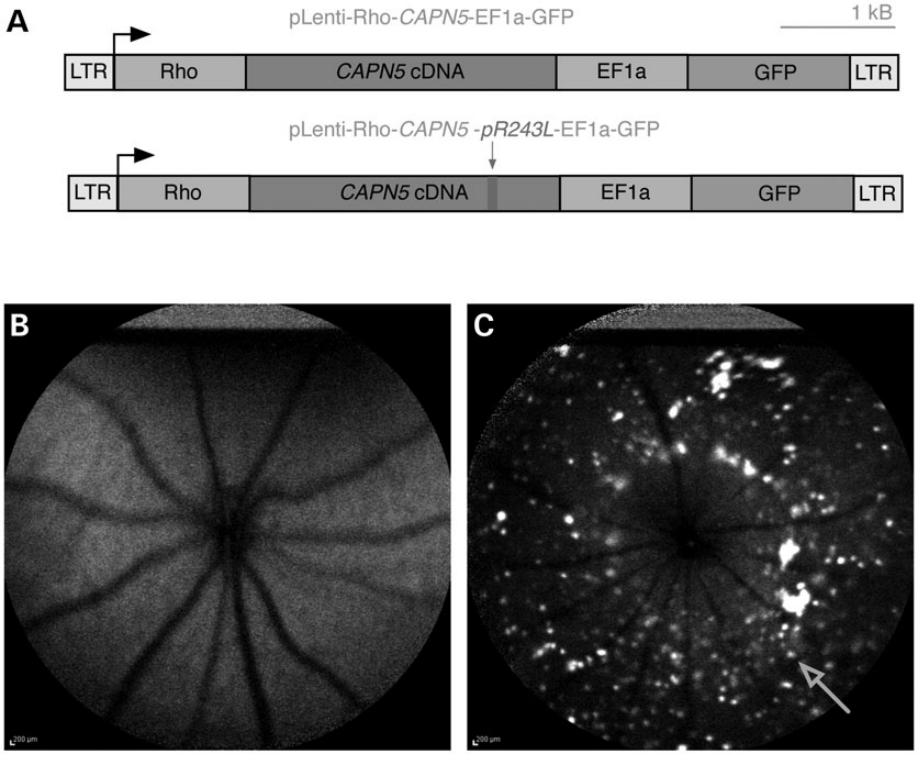

Figure 4. Expression of lentiviral construct after subretinal injection in mice. (**A**) Lentiviral construct map of wild-type human (h) *CAPN5* and mutant ADNIV h*CAPN5*-R243L with green fluorescent protein (GFP) tag. (**B**) Autofluorescence fundus image at 5 months of age of a B6 non-injected eye, and (**C**) the fellow B6 eye that was injected at post-natal day 5 with the wild-type h*CAPN5* lentivirus showing punctate GFP expression (arrow). LTR, long terminal repeat; Rho, mouse rhodopsin promoter; EIFa, elongation factor promoter.

groups. This suggests that there may be a mild loss of visual function associated with the overexpression of human calpain-5 in the mouse eye, as seen with the *hCAPN5* wild-type lentivirus transductions, but a stronger phenotype in the mice that received an injection with the single amino acid mutation: *hCAPN5-R243L*.

Examination of the photoreceptor-specific *a*-wave amplitudes in the dark-adapted 3.0 maximal combined ERG visual responses displayed a mild loss of the photoreceptor cell response in the eyes injected with saline (blue), the wild-type *hCAPN5* lentivirus (green) and the mutant *hCAPN5-R243L* lentivirus (red), but not in the eyes injected with the control GFP lentivirus (Fig. 5F). This may be due to the surgical injection procedure, which has been previously reported by Wert *et al.* to cause a slight reduction in *a*-wave amplitude in the mouse (18). However, the eyes injected with either saline

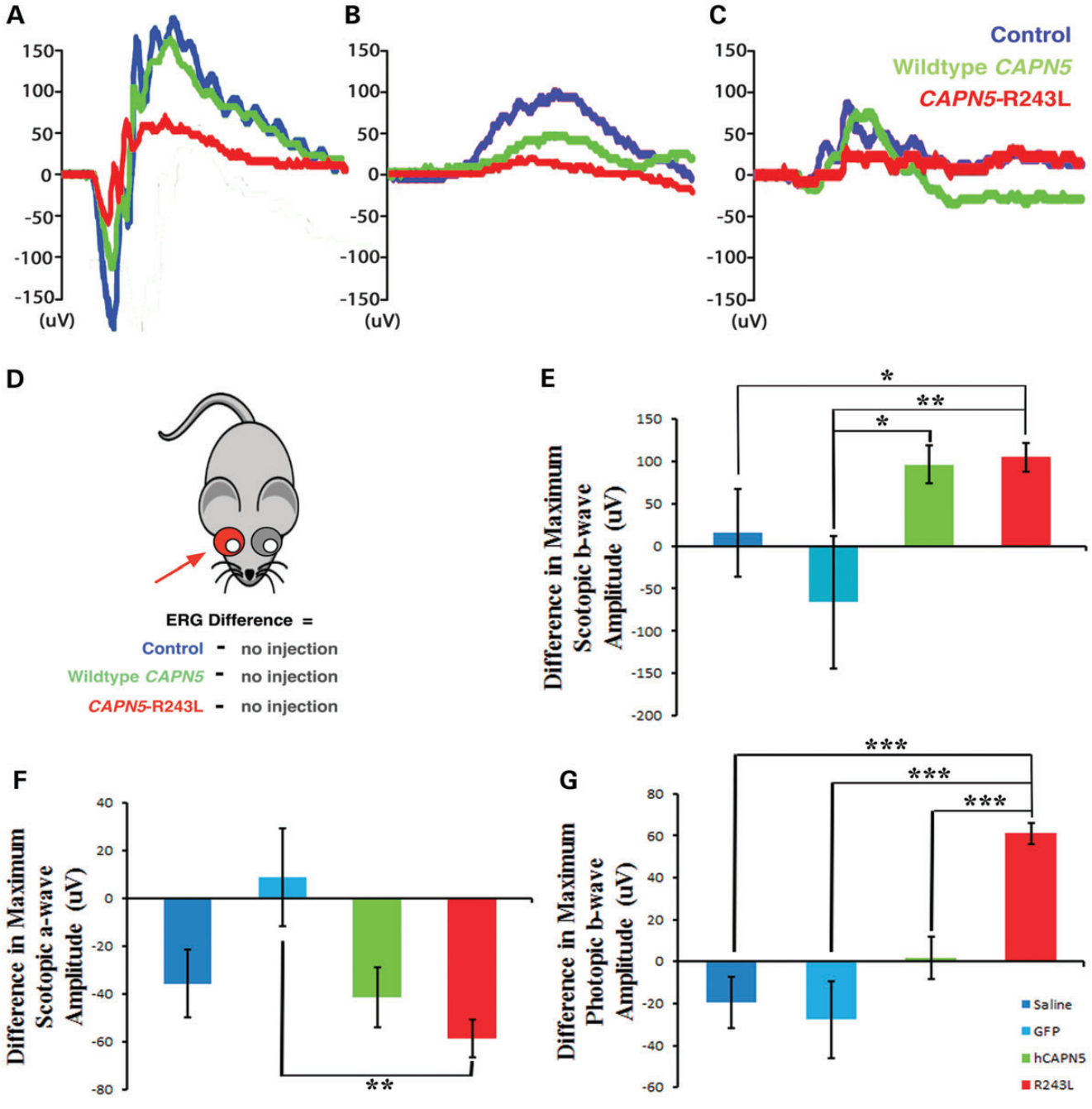

Figure 5. Electroretinography shows reduced visual function in retinas injected with mutant *CAPN5* lentiviral vector. (**A**) Representative traces of scotopic rod-cone maximum ERG responses at 3 months of age in control (blue), *hCAPN5* (green) and *hCAPN5-R243L* (red) mice. (**B**) Representative traces of scotopic dim-light rod-only ERG responses at 3 months of age in control (blue), *hCAPN5* (green) and *hCAPN5-R243L* (red) mice. (**C**) Representative traces of photopic cone-specific ERG responses at 3 months of age in control (blue), *hCAPN5* (green) and *hCAPN5-R243L* (red) mice. (**D**) Cartoon depicting the injected eye of the mouse and uninjected fellow eye, with colors corresponding to injected solution (blue, control saline or GFP lentivirus without transgene; green, wild-type *hCAPN5* lentivirus; red, ADNIV mutant *hCAPN5-R243L* lentivirus). (**E**) Differences between the injected (dark blue, saline; light blue, GFP lentiviral vector without transgene; green, wild-type *hCAPN5* lentiviral vector; red, mutant *hCAPN5-R243L* lentiviral vector) and uninjected eyes for scotopic maximum rod-cone *b*-wave amplitudes at 3 months of age. (**F**) Differences between the injected (dark blue, saline; light blue, GFP lentiviral vector without transgene; green, wild-type *hCAPN5* lentiviral vector; red, mutant *hCAPN5-R243L* lentiviral vector) and uninjected eyes for scotopic maximum rod-cone *a*-wave amplitudes at 3 months of age. (**G**) Differences between the injected (dark blue, saline; light blue, GFP lentiviral vector without transgene; green, wild-type *hCAPN5* lentiviral vector; red, mutant *hCAPN5-R243L* lentiviral vector) and uninjected eyes for photopic, cone-specific *b*-wave amplitudes at 3 months of age. Statistical significance analyzed for difference between groups using a paired *t*-test analysis ($^{*}P < 0.05$; $^{**}P < 0.01$; $^{***}P < 0.001$). $n = 3, 3, 10$ and 19 for the saline, GFP lentivirus, *hCAPN5* lentivirus and *hCAPN5-R243L* lentivirus-injected eyes, respectively.

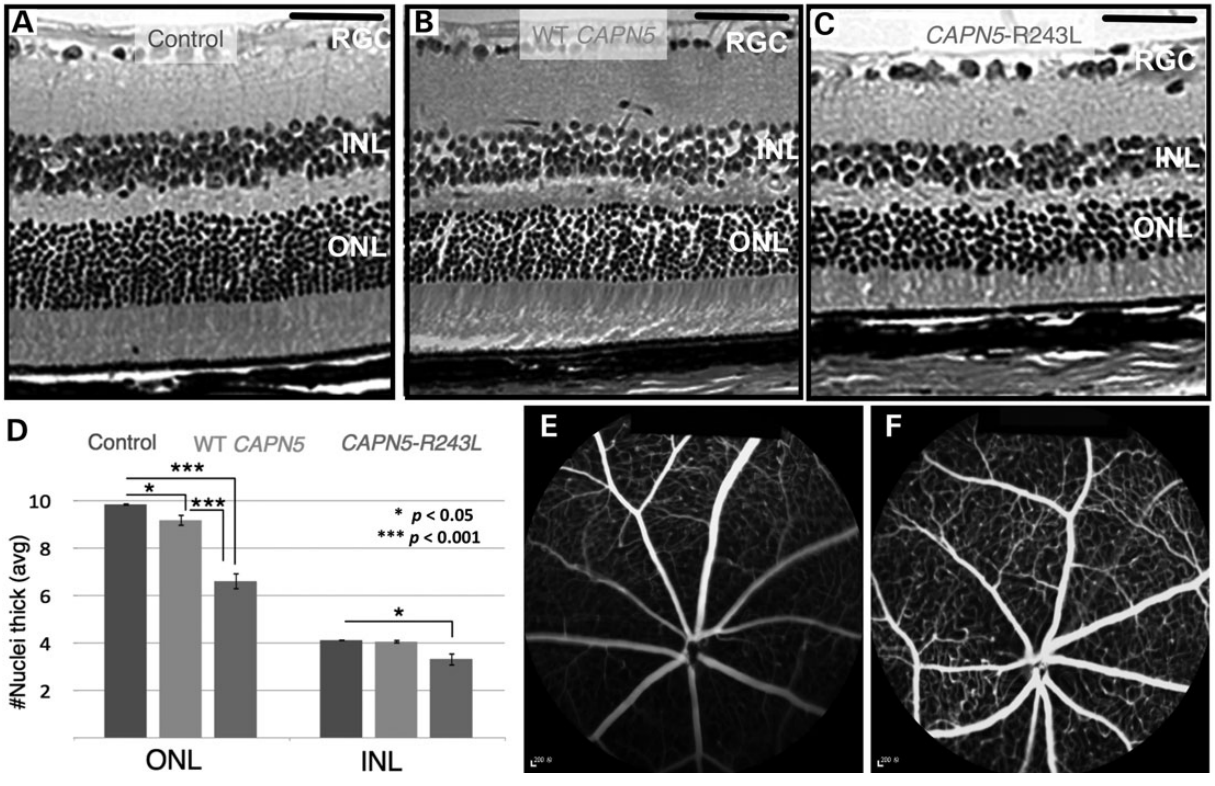

Figure 6. Photoreceptor degeneration after mutant *CAPN5* overexpression. (**A**) Retina of a hematoxylin and eosin (H&E)-stained wild-type B6 control mouse eye at 6 months of age, (**B**) a wild-type *hCAPN5* lentiviral-injected eye and (**C**) a mutant *hCAPN5-R243L* lentiviral-injected eye. Scale bar = 600 μm. RGC, retinal ganglion cells; INL, inner nuclear layer; ONL, outer nuclear layer. (**D**) Quantification of outer nuclear layer (ONL) and inner nuclear layer (INL) thickness in control, *hCAPN5* lentiviral-injected and mutant *hCAPN5-R243L* lentiviral-injected eyes at 6 months of age. $^{*}P < 0.05$; $^{***}P < 0.001$. $n \geq 4$ mice. (**E**) Fluorescein angiography of a B6 eye injected with the mutant *hCAPN5-R243L* lentivirus compared with (**F**) the uninjected fellow eye.

(blue) or the wild-type *hCAPN5* lentivirus (green) had a similar loss of the *a*-wave amplitude (-35.8 ± 14.2 μV and -41.3 ± 12.5 μV, respectively), whereas the eyes injected with the mutant *hCAPN5-R243L* lentivirus had a statistically significant loss of the photoreceptor visual response in comparison with the GFP lentivirus controls, and a greater loss of photoreceptor response overall (-58.6 ± 8.0 μV).

Although the lentiviral vector targeted rods, the cone-specific photopic ERG responses gave a result specific to the single R243L amino acid mutation. The two control groups (blue) and the wild-type *hCAPN5* lentivirus (green) did not reduce cone cell visual function in the injected eyes (Fig. 5G). However, the mutant *hCAPN5-R243L* lentivirus (red) caused a statistically significant reduction in cone cell function compared with all three other groups, with a loss of 61.2 ± 5.0 μV (Fig. 5G). Overall, the ERG differences between the injected and uninjected eyes for the entire cohort of mice displayed a cone and inner retina cell loss of function after injection with the *hCAPN5-R243L* lentivirus that was not found in the other three groups analyzed, and therefore specific to the single R243L amino acid change.

hCAPN5-R243L causes a reduction in the number of photoreceptor cells in the mouse retina

In the later stages of ADNIV, patients show signs of photoreceptor degeneration, inflammatory cell infiltrates, retinal fibrosis and neovascularization. These phenotypes were ascertained 6 months following injection of the viral vectors. Compared with uninjected mouse eyes (Fig. 6A), the eyes injected with *hCAPN5* lentivirus showed a mild decrease in number of photoreceptor cell nuclei (Fig. 6B). The photoreceptor IS and OS and the inner nuclear layer (INL) appeared similar to the uninjected control eyes (Fig. 6A and B). In contrast, eyes injected with the ADNIV mutant *hCAPN5-R243L* displayed a greater loss of photoreceptor cell nuclei and a significant shortening of the photoreceptor IS and OS (Fig. 6C) in comparison with both the uninjected eyes and the eyes injected with *hCAPN5* (Fig. 6A and B). Additionally, a decrease in the INL was visible in the *hCAPN5-R243L* lentivirus-injected eyes (Fig. 6C), which was not present in the uninjected eye or the eye injected with *hCAPN5* (Fig. 6A and B) or the GFP-only vector (data not shown). This correlated with the earlier loss of the combined maximum ERG *b*-wave amplitude and the loss of the photopic ERG *b*-wave amplitude that was greater in only the eyes injected with the ADNIV mutant lentivirus, supporting a disease-causing effect of the R243L amino acid change. This level of photoreceptor loss is sufficient to result in significantly greater ERG loss, as observed in late-stage ADNIV patients.

Quantification of cell nuclei of the outer and inner nuclear layer (ONL and INL, respectively) was performed. The *hCAPN5-R243L*-injected eyes were compared with the *hCAPN5*-injected eyes and the uninjected fellow eyes. ONL thickness was reduced in both the *hCAPN5* lentivirus-injected eyes and the *hCAPN5-R243L* lentivirus-injected eyes (Fig. 6D). However,

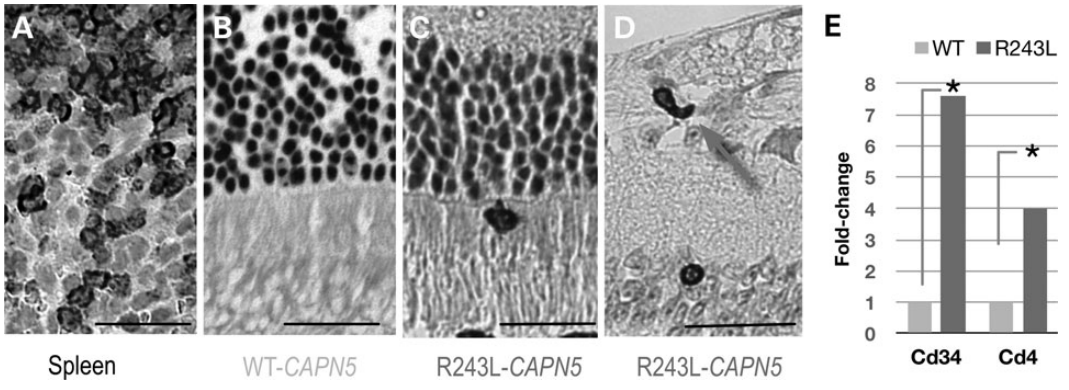

Figure 7. T-cell-related markers in the retina after subretinal injection of mutant CAPN5 lentiviral vector. (**A**) Immunohistochemistry of CD3-positive T cells in spleen. (**B**) Wild-type *hCAPN5* lentiviral-injected eye had no CD3-positive cells present. (**C** and **D**) *hCAPN5-R243L* lentiviral-injected eyes had several CD3-positive cells in immunohistochemistry labeled sections (arrows). (**E**) T-cell markers, CD34 and CD4, are up-regulated in the *hCAPN5-R243L* retinas compared with the wild-type *hCAPN5* retinas (* $P < 0.05$).

there was a significantly greater reduction in the ONL of the eyes injected with the *hCAPN5-R243L* allele. These eyes also had an additional significant loss of the INL that was not found in the wild-type *hCAPN5* lentivirus-injected eyes (Fig. 6D). Each localized region of retinal tissue loss correlated with sites of calpain-5 expression and ERG results (Figures 3 and 5). This included the calpain-5 detected in the OPL of both mouse and human retina (Fig. 3). This could explain the loss of INL cells.

In this mouse model, ERG signaling defects preceded photoreceptor degeneration similar to the human disease. Histological examination of the mutant mouse eyes did not identify neovascularization, epiretinal membranes or vitreous membranes (data not shown) that are found in latest stages of ADNIV. Fluorescein angiography did not detect any retinal vascular leakage, vascular remodeling or neovascularization (Fig. 6E) compared with the uninjected fellow eye (Fig. 6F).

Expression of *hCAPN5-R243L* up-regulates local inflammatory responses

Uveitis in ADNIV patients is characterized by infiltrating CD3+ and CD4+ inflammatory cells in the vitreous, the iris and the retina (4,11,19,20). We performed immunohistochemistry (IHC) on serial sections of injected mouse retinas to identify CD3+ cells. Spleen CD3+ cells were used as a positive control (Fig. 7A). No CD3+ cells were detected in the eyes of mice injected with the *hCAPN5* lentivirus (Fig. 7B), or in saline and GFP-only control injected eyes (data not shown). However, scattered CD3+ cells were detected in the retinas of the *hCAPN5-R243L* lentivirus-injected eyes (Fig. 7C and D). CD3+ cells were present in these eyes in the photoreceptor cell IS and OS (Fig. 7C) and traversing the retinal blood vessels (Fig. 7D; arrow). This distinction between the wild-type *hCAPN5* and mutant allele suggested that simple overexpression was insufficient to elicit an ADNIV immune response, but other molecular pathways might be activated by the mutant. The cellular immune response was limited compared with human ADNIV patients, and no CD3+ cells were found in the vitreous or iris.

To determine whether the disease allele caused a unique molecular response compared with the normal allele, we surveyed 84 retinal transcripts for T-cell-related markers, inflammatory cytokines and chemokines using qPCR arrays, because there was not sufficient tissue for protein assays. Mouse retinal cDNA from eyes injected with the *hCAPN5* lentivirus was compared with the eyes injected with the *hCAPN5-R243L* lentivirus. The hematopoietic progenitor cell antigen CD34 is expressed by vascular endothelial cells and typically required for T-cell recruitment. We found that both CD34 and CD4 T-cell expression marker were significantly up-regulated in the eyes injected with the *hCAPN5-R243L* (Fig. 7E; red) compared with the eyes injected with *hCAPN5* (Fig. 7E; green). Other markers associated with T cells, such as CD8 and *Foxp3*, were not differentially expressed (data not shown), suggesting the presence of effector T cells but not regulatory T cells.

In addition to T cells, retinal cells are a local source of inflammatory gene expression in the eye. A few cytokines and chemokines were differentially expressed in the eyes injected with the *hCAPN5-R243L* compared with the eyes injected with *hCAPN5.* Two other chemokines, C-C motif ligand 7 and C-C motif chemokine 22, also had significantly altered expression in the eyes that received the mutant allele (Fig. 8). Although these chemokines were differentially expressed, no change in expression of their receptor, chemokine receptor 6 (*Ccr6*), was detected. Chemokine C-X3-C motif ligand 1 (*Cx3cl1*), a T-cell attractant, was significantly decreased (Fig. 8).

We found that IL-12 transcript was significantly increased in the eyes injected with the *hCAPN5-R243L* mutant allele compared with the eyes injected with the *hCAPN5* wild-type allele (Fig. 8). Il-12 is necessary for the differentiation of T cells into Th17 cells, which are associated with autoimmunity. This finding correlates with cytokine expression in human ADNIV eyes (unpublished observation). Colony-stimulating factor 3 (*Csf3*), an inducer of neurogenesis and anti-apoptotic protein in the central nervous system, was decreased in the eyes injected with the *hCAPN5-R243L* lentivirus compared with the wild-type *hCAPN5* lentivirus. In contrast, interleukin-10 (IL-10), an anti-inflammatory cytokine, had no difference in expression (Fig. 8). This again supports the absence of T-regulatory cell pathway in the mouse ADNIV model.

We also observed changes in transcriptional proteins associated with inflammation. *Socs3*, a suppressor of cytokine signaling, was

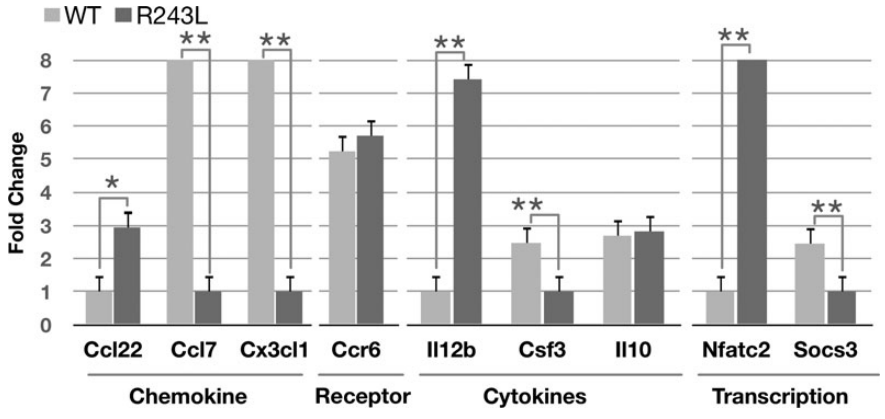

Figure 8. Inflammatory gene expression after subretinal injection of mutant CAPN5 lentiviral vector. Retinas from *hCAPN5-R243L*-injected mice were compared with the wild-type *hCAPN5*-injected mouse retinas using real-time quantitative PCR arrays. Four mice were analyzed for each condition. Up-regulation of cytokines such as *Il-12b* suggests a Th17 differentiation pathway, where *Il-10* would have suggested regulatory T-cell (Treg) differentiation but was found unchanged. The transcription factor, *Nfatc,* was increased in the mutant injected retina. Some genes were down-regulated including *Ccl2, Cx3cl1, Csf3* and *Socs3.* Normalized samples were analyzed in triplicate, and the SEM was on average only 1.1% of the total average Ct values per condition ($^{*}P < 0.05$, $^{**}P < 0.01$).

decreased in the eyes that received the mutant ADNIV allele (Fig. 8). Nuclear factor of activated T cells, cytoplasmic 2 (*Nfatc2*), was increased in the eyes with the mutant *hCAPN5-R243L* allele compared with eyes with the wild-type *hCAPN5* allele (Fig. 8). This gene is responsible for inducing gene transcription changes during an immune response. Interestingly, the *Nfatc* pathway is activated by other calpain isoform activity (21).

Despite the limited number of CD3+ cells infiltrating the retina, there were significant differences in the expression of T-cell markers, cytokines, chemokines and transcription factors in the eyes injected with the *hCAPN5-R243L* lentivirus compared with the *hCAPN5* lentivirus, all of which influence a number of downstream genes and signaling pathways.

DISCUSSION

We engineered a mouse model using a mutant disease allele of *CAPN5* and examined this model for the early and/or late features of human ADNIV. The eyes were tested for changes in the ERG, retinal degeneration and the presence of inflammatory cells, fibrosis and neovascularization. Our study shows that the c.728G>T, p.Arg243Leu mutation in calpain-5 causes both early (CD3+ T-cell migration into the retina and reduction in ERG *b*-wave amplitudes) and later (photoreceptor degeneration and altered inflammatory gene expression) features of ADNIV in mice. There is evidence of retinal inflammation correlating with the human uveitis. There was no evidence of retinal neovascularization or intraocular fibrosis characteristic of end-stage human disease, but the mice were only examined for 6 months. Subretinal injection of the lentiviral vectors limits expression to only ~20% of the retina (Fig. 4C), so a more robust phenotype might be observed in a transgenic model in which all photoreceptors express mutant *CAPN5*, like the human ADNIV patients.

Our lentiviral constructs included a rhodopsin promoter, driving the expression of either the wild-type *hCAPN5* or the mutant *hCAPN5-R243L* specifically within the rod photoreceptor cell. Calpain-5 expression in the mouse retina correlated with expression of the protein in the human retina. Calpain-5 was found to be located in the inner and outer segments (IS and OS, respectively) of the photoreceptor cells, and also within the outer plexiform layer (OPL). In the rod cells, overexpression of *hCAPN5* or the expression of the mutant *hCAPN5-R243L* within the photoreceptor synapse (OPL) and the photoreceptor outer and inner segments causes an early loss of signaling before noticeable degeneration of the photoreceptor cells. The early loss of the inner retina signaling at 3 months, in the absence of cell degeneration, correlates with a potential defect in OPL synaptic signal transduction from the photoreceptor to the inner nuclear layer.

The *hCAPN5-R243L* mutation caused the strongest effect in the loss of the cone cell function compared with the other lentiviral vectors and the saline control group. Our lentiviral constructs used a rhodopsin (rod cell-specific) promoter. A leaky promoter is one possible explanation, but this seems unlikely because we have not observed this effect in other transgenic mice. It is well established that rod photoreceptor degenerative diseases eventually lead to the death of the cone cells in retinitis pigmentosa (22,23). Therefore, the decline in cone cell function could represent a non-autonomous cell effect caused by the release of secreted cytokines or inflammatory effectors from mutant *CAPN5* in rods. The cones tend to be more severely affected in comparison with the rods in human retinal inflammatory diseases (24). The decline of cone cell function after transduction of the ADNIV mutant allele into the rod cells may cause secondary cone cell degeneration detectable with ERG analysis as early as 3 months of age. This finding remains to be explored in humans but could be an early clinical sign of disease.

Histological analysis supports both the localization of calpain-5 and the ERG function results. The mutant *hCAPN5-R243L*-injected eyes displayed a significantly greater loss of the outer nuclear layer (ONL) than the wild-type *hCAPN5*-injected eyes, along with a shortening of the IS and OS. *hCAPN5-R243L*-injected eyes also had a significant loss of the inner nuclear layer (INL) that was not seen in the wild-type *hCAPN5*-injected eyes. This corresponds to the localization of calpain-5 in the outer plexiform layer (OPL) found in both the mouse and human retinas. The localization of calpain-5 in this

layer was not previously reported. However, this statistically significant loss of cellular thickness in the INL may explain the inner retina ERG deficiency that is found early in human ADNIV patients.

The molecular mechanisms that initiate neuroinflammation are poorly understood, and ADNIV provides a genetic model for investigation. The ADNIV mouse model showed evidence of retinal inflammation correlating with the human uveitis. This makes the model unique, because most models of eye inflammation use LPS or peptides to artificially induce uveitis in mice (25,26). There was no evidence of retinal neovascularization or intraocular fibrosis characteristic of end-stage human disease; however, CD3+ T cells were detected within the retina similar to the findings in human ADNIV eyes. Furthermore, we detected an up-regulation of several cytokines, chemokines and transcription factors related to inflammation after subretinal injection with the mutant *hCAPN5-R243L* lentiviral vector, in comparison with eyes injected with the wild-type *hCAPN5* lentiviral vector. This retina-only expression of mutant *hCAPN5-R243L* was sufficient to generate an inflammatory response in our pre-clinical ADNIV mouse model. Calpains are also expressed in T cells, and mutating *CAPN5* within the T cells, as well as within the retina, may provide a more robust inflammatory phenotype. It is also possible that cytokines may be generated by this R243L mutation locally from the retina to recruit the inflammatory cells, because calpains have been shown to cause necrotic cell death. For example, *Tra-3* (the calpain-5 homolog in *c. elegans*) is responsible for neuronal degeneration (5).

The effects of subretinal injections are typically localized near the site of the subretinal bleb and are known to affect ~20–30% of the cells of the retina (18,27). Therefore, an autoimmune response to the presence of the mutant lentivirus would be confined to 20–30% of the retina where the injection site was located in the wild-type mice and may limit the extent of inflammatory triggers within these retinas. The presence of even limited numbers of T cells and altered inflammatory gene expression suggests that in a transgenic mouse model of *hCAPN5-R243L*, the autoimmune response would most likely be present throughout the retina. Additionally, both ERG visual function loss and the loss of the photoreceptor cell and inner nuclear layer of the eye may be limited owing to the confines of the lentivirus to the location of the subretinal bleb. It would be expected that the lentiviral injections will lead to a less severe decline in ERG response and cellular degeneration than would be expected in a transgenic mouse model. Therefore, a transgenic mouse carrying the R243L-mutated *hCAPN5* allele would be useful for future modeling of human ADNIV disease.

Although a transgenic model may have a more severe disease phenotype, both human ADNIV patients and the *hCAPN5-R243L* lentiviral model displayed a decline in visual response, particularly with the cone and inner retinal cells, photoreceptor degeneration within both the ONL and INL, and the presence of T cells and altered inflammatory gene expression. This strongly supports that the R243L amino acid change found in human ADNIV patients is a disease-causing mutation. The *hCAPN5-R243L* disease allele is able to recapitulate aspects of the human ADNIV phenotype in wild-type mice. Retinal expression of this disease-causing allele is sufficient for ERG functional deterioration and appears to trigger a T-cell response against the retina. Taken together, our studies suggest that ADNIV is due to *CAPN5* gain-of-function and that retinal expression may be sufficient to generate an autoimmune response. Moreover, genetic models of ADNIV can be developed in the mouse and serve as pre-clinical models for therapeutic testing. The finding that inhibition of calpain activity can rescue other forms of photoreceptor degeneration suggests that this model may be valuable in other retinal diseases (28–31).

MATERIALS AND METHODS

Human ADNIV case

The collection of data used in this study was approved by the Institutional Review Board for Human Subjects Research at the University of Iowa, was compliant with the Health Insurance Portability and Accountability Act and adhered to the tenets of the Declaration of Helsinki. Clinical examination and testing was performed as previously described (32). Stereoscopic color fundus images and autofluorescent (AF) images were obtained using a Topcon TRC 50DX camera (Topcon, Pyramus, NJ, USA). Optical coherence tomography imaging was obtained from the spectral-domain Heidelberg HRA2 Spectralis, version 1.6.1 (Heidelberg Engineering, Inc, Vista, CA, USA). A full-field electroretinogram was performed using DTL recording electrodes and Ganzfeld stimulation according to international standards, as previously described (11). Briefly, the eyes were dilated and dark-adapted for 30 min. Electroretinograms were recorded simultaneously from both eyes using Burian-Allen bipolar contact lens electrodes. Evoked waveforms, a 100-μV calibration pulse, and a stimulus artifact were recorded on Polaroid film (11). Genetic testing was performed as previously described (4).

Mouse lines and husbandry

C57BL/6J mice were obtained from the Jackson Laboratory (Bar Harbor, ME, USA). Mice were maintained in the Columbia University Pathogen-free Eye Institute Annex Animal Care Services Facility under a 12/12-h light/dark cycle. All experiments were approved by the local Institutional Animal Care and Use Committee (IACUC). Mice were used in accordance with the Statement for the Use of Animals in Ophthalmic and Vision Research of the Association for Research in Vision and Ophthalmology, as well as the Policy for the Use of Animals in Neuroscience Research of the Society for Neuroscience.

Immunofluorescence

Sections were deparaffinized and rehydrated to dH_20. Antigen retrieval was performed using 10 mM citrate buffer (pH 6.0) in a 650-watt microwave. Slides were microwaved for 5 min, cooled for 5 min, microwaved for 5 min, cooled for 30 min and then rinsed in PBS 3 × 3 min. Sections were permeabilized using 0.1% Triton X-100 in PBS (pH 7.4) for 10 min, followed by another 3 × 3 min rinses in PBS. Sections were blocked in 5% normal goat sera (G-9023, Sigma) for 2 h. Primary antibody incubation using 4 μg/ml rabbit anti-calpain5 (ab38943, Abcam) or normal rabbit IgG as a control, diluted in block, was performed overnight at 4°C. Sections were rinsed 3 ×

3 min in PBS and then incubated with 1.2 μg/ml goat anti-rabbit IgG-biotin-conjugated antibody (111-066-047, Jackson ImmunoResearch) for 30 min at RT. Sections were rinsed and incubated with streptavidin-Alexa 647 fluorescent conjugate (S11223, Invitrogen) diluted 1/500 in blocking solution for 1 h and then rinsed again. Slides were mounted with VectaShield containing DAPI (H-1200, Vector Laboratories). Images were collected using a Zeiss 710 confocal microscope with 405 nm and 633 nm excitation for nuclei and anti-calpain5, respectively.

RNA preparation and next-generation sequencing

Total RNA was extracted from mouse retinas using RNAeasy (Qiagen) and submitted to Otogenetics Corporation (Norcross, GA USA) for RNA-Seq assays. Briefly, the integrity and purity of total RNA were assessed using Agilent Bioanalyzer and OD260/280. One to two micrograms of cDNA was generated using Clontech SmartPCR cDNA kit (Clontech Laboratories, Inc., Mountain View, CA, USA, catalog# 634925) from 100 ng of total RNA, and adaptors were removed by digestion with RsaI. The resulting cDNA was fragmented using Covaris (Covaris, Inc., Woburn, MA, USA), profiled using Agilent Bioanalyzer and subjected to Illumina library preparation using NEBNext reagents (New England Biolabs, Ipswich, MA, USA, catalog# E6040). The quality and quantity and the size distribution of the Illumina libraries were determined using an Agilent Bioanalyzer 2100. The libraries were then submitted for Illumina HiSeq2000 sequencing according to the standard operation. Paired-end 90- or 100-nucleotide (nt) reads were generated and checked for data quality using FASTQC (Babraham Institute, Cambridge, UK) and subjected to data analysis using the platform provided by DNAnexus (DNAnexus, Inc, Mountain View, CA, USA) or the platform provided by Center for Biotechnology and Computational Biology (University of Maryland, College Park, MD, USA) as previously described (Nature Protocols 7: 562–578, 2012).

Construction of lentiviral vectors

The *CAPN5* gene and its mutations in an Origene vector were cut with SalI/AscI and then ligated into a lentiviral vector cut with XhoI/AscI. The promoter driving the *CAPN5* gene and its mutated versions is 2.0 kilobases of the mouse rhodopsin promoter upstream of the *hCAPN5* or *hCAPN5-R243L* gene. The host lentiviral vector contains a cassette of EF1a-GFP, so it co-expresses GFP. The lentiviral vectors also contained a 5′ long terminal repeat (LTR), a packaging signal (ψ), a transfer (t)RNA primer binding site, a reverse response element and a 3′ LTR. Lentiviral particles were packaged by co-transfecting the above-mentioned lentiviral construct with the R8.91 helper plasmid and a VSV-G plasmid to created self-inactivating viral vectors (Biogenova Corporation, Frederick, MD, USA). The ratio of plasmids used for transfection is 1 : 1.5 : 0.5, respectively. The packaging cell line was 293 T cells. Ten 180-mm tissue culture flasks were used, and 250 ml of the viral packing supernatant was collected. Lentiviral particles were purified and concentrated using the Biogenova proprietary viral purification technology. The viral titer was determined by transducing 293 T cells by the viral supernatant with a limiting dilution assay. Each GFP-positive clone was counted as one transfection unit (TU) under a fluorescence microscope on the third day after virus transduction.

Transduction of lentiviral vectors

We injected 0.7 μl of $\sim 2.0 \times 10^7$ transfection units (TU)/ml into the subretinal space of the right eye of *C57BL/6J* mice at post-natal day (P) 5. The subretinal injection was performed as previously described (18,27,33). Virus particles were injected at the 6-o'clock position of the eye, ∼1.5 mm from the limbus, to produce a subretinal bleb in the mid-periphery of the retina. The left eyes of all mice were kept as a matched control for experimental analyses. Anesthesia and surgery were performed as previously described (12).

Autofluorescence imaging

For the mice, AF fundus imaging was obtained with the Spectralis scanning laser confocal ophthalmoscope (OCT-SLO Spectralis 2; Heidelberg Engineering, Heidelberg, Germany). Pupils were dilated using topical 2.5% phenylephrine hydrochloride and 1% tropicamide (Akorn, Inc., Lakeforest, IL, USA). Mice were anesthetized by intraperitoneal injection of 0.1 ml/10 g body weight of anesthesia [1 ml ketamine—100 mg/ml (Ketaset III, Fort Dodge, IA, USA) and 0.1 ml xylazine—20 mg/ml (Lloyd Laboratories, Shenandoah, IA, USA) in 8.9 ml PBS]. Body temperature was maintained at 37°C using a heating pad during the procedure. AF imaging was obtained at 488-nm absorption and 495-nm emission using a 55° lens. Images were taken of the central retina, with the optic nerve located in the center of the image.

Electroretinograms

Mice were dark-adapted overnight, manipulations were conducted under dim red light illumination and recordings were made using Espion ERG Diagnosys equipment (Diagnosys LLL, Littleton, MA, USA). Adult B6 control mice were tested at the beginning of each session to ensure equal readouts from the electrodes for both eyes before testing the experimental mice. Pupils were dilated using topical 2.5% phenylephrine hydrochloride and 1% tropicamide (Akorn, Inc.). Mice were anesthetized by intraperitoneal injection of 0.1 ml/10 g body weight of anesthesia [1 ml ketamine—100 mg/ml (Ketaset III) and 0.1 ml xylazine—20 mg/ml (Lloyd Laboratories) in 8.9 ml PBS]. Body temperature was maintained at 37°C using a heating pad during the procedure. Hand-made electrodes were placed upon the corneas, and gonioscopic prism solution (Alcon Labs, Inc., Fort Worth, TX, USA) was applied to each eye. Both eyes were recorded simultaneously. A total of 40–60 responses were averaged for each trial. All further detail on the ERG method has been described previously (34,35). We measured scotopic maximal b-wave ERG responses to assess inner retina function, scotopic maximal a-wave ERG responses to assess photoreceptor-specific function and photopic maximal b-wave ERG responses to assess cone-specific function. Maximal responses were taken from the Espion readout in microvolts and quantified using paired *t*-test statistical analyses with statistical significance set at $P < 0.05$. Three out of the twenty-two mice injected with the *hCAPN5-R243L* mutant

lentivirus were excluded from the final ERG analysis, because they were outliers that did not show any difference between the uninjected and injected eyes whereas a strong statistically significant loss of ERG function for the inner retina and cone cells was found in the other 19 injected mice (see Results); it is likely that the virus was not correctly injected into the subretinal space of the eye in these three mice.

Histochemical analyses

Mice were sacrificed and the eyes enucleated as previously described (36). Excalibur Pathology, Inc. (Oklahoma City, OK) prepared Hematoxylin & Eosin retinal sections. The morphology of photoreceptors and the amount of photoreceptor cell nuclei of lentiviral-treated eyes were compared with the untreated fellow eyes. Quantification of photoreceptor nuclei was conducted on several sections that contained the optic nerve, as follows: the distance between the optic nerve and the ciliary body was divided into four, approximately equal, quadrants. Three columns of nuclei (how many cell nuclei thick) were counted within each single quadrant. These counts were then used to determine the average thickness of the ONL for each individual animal at each time. Averages and standard deviations were calculated from animals for each time point using *t*-test statistical analyses with statistical significance set at $P < 0.05$. Sectioning proceeded along the long axis of the segment, so that each section contained upper and lower retina as well as the posterior pole.

Angiography

Fluorescein angiography was obtained with the Spectralis scanning laser confocal ophthalmoscope (OCT-SLO Spectralis 2; Heidelberg Engineering). Pupils were dilated using topical 2.5% phenylephrine hydrochloride and 1% tropicamide (Akorn, Inc.). Mice were anesthetized by intraperitoneal injection of 0.1 ml/10 g body weight of anesthesia [1 ml ketamine—100 mg/ml (Ketaset III) and 0.1 ml xylazine—20 mg/ml (Lloyd Laboratories) in 8.9 ml PBS]. Body temperature was maintained at 37°C using a heating pad during the procedure. And 0.05 ml of 10% AK-Flour (100 mg/ml, Akorn, Inc.) was injected intra-peritoneally after anesthesia. Imaging was obtained at 488-nm absorption and 495-nm emission using a 55° lens. Images were taken of the central retina, with the optic nerve located in the center of the image.

Immunohistochemistry

Twelve eyes representing the injected GFP control, wild-type *hCAPN5*, mutant *hCAPN5-R243L*, and no injected fellow eyes were serially sectioned, along with ten wild-type eyes. Sections were deparaffinized in xylenes, rehydrated in graded alcohols to distilled water. Antigen retrieval was accomplished using citrate buffer pH 9.0 in a decloaking chamber (Biocare). Endogenous peroxidase activity was quenched with 3% hydrogen peroxide solution for 8 min. Sections were rinsed in distilled water and washed 5 × 2 min. Sections were incubated with anti-CD3 antibody diluted 1/100 (RM-91070S, Neomarkers) for 30 min at RT followed by a buffer wash. DAKO Mouse Envision HRP System reagent was applied to slides and allowed to incubate for 30 min at RT. Slides were washed in buffer and developed with DAKO DAB Plus for 5 min followed by DAB Enhancer for 3 min. Slides were rinsed in distilled water, counterstained and coverslipped. Sections were also immunolabeled using a polyclonal anti-calpain 5 primary antibody (Santa Cruz Biotechnology, Inc., Santa Cruz, CA), AlexaFluor 488 donkey anti-rabbit secondary antibody (Invitrogen, Carlsbad, CA) and 4′,6-diamidino-2-phenylindole (DAPI; Invitrogen). Images were captured with a Zeiss LSM 710 equipped with Zen2009 software (Zeiss, Germany).

Human donor tissue was received from the Iowa Lions Eye Bank (Iowa City, IA). Tissue was dissected and fixed in 4% paraformaldehyde (pH 7.4). Sections cut 7 μm thick were immunolabeled using a polyclonal anti-calpain 5 primary antibody (Abcam), AlexaFluor 488 donkey anti-rabbit secondary antibody (Invitrogen) and 4′,6-diamidino-2-phenylindole (DAPI; Invitrogen). Images were captured with a Zeiss LSM 710 equipped with Zen2009 software (Zeiss, Germany).

Real-time PCR array analysis

Mouse retinas were isolated as previously described (37). RNA was extracted from the cells as described earlier and reverse-transcribed using the RT^2 First Strand Kit according to manufacturer's instructions (SABiosciences/Qiagen, Valencia, CA, USA). Mouse cDNA was added to SABiosciences RT^2 qPCR master mix and then added to the 96 wells of the mouse Th17 Response RT^2 Profiler PCR Array System (Product # PAMM-073Z-A; SABiosciences/Qiagen). Quantitative PCR was performed using the Applied Biosystems Model 7000 sequence detection system (Applied Biosystems, Inc., Foster City, CA).

AUTHORS' CONTRIBUTIONS

K.J.W., J.M.S., S.H.T. and V.B.M. designed the research; K.J.W., A.K.O, and J.M.S. performed the research; K.J.W., J.M.S., S.H.T., A.G.B. and V.B.M. analyzed the research; K.J.W., J.M.S., A.G.B., S.H.T. and V.B.M. wrote the paper.

Conflict of Interest statement. None declared.

FUNDING

This work was supported by the National Institute of Health Core (5P30EY019007), National Cancer Institute Core (5P30CA013696) and unrestricted funds from Research to Prevent Blindness, New York, NY, USA. S.H.T. is a member of the RD-CURE Consortium and is supported by Tistou and Charlotte Kerstan Foundation, the National Institute of Health (R01EY018213), the Research to Prevent Blindness Physician-Scientist Award, the Barbara and Donald Jonas Family Fund, and the Foundation Fighting Blindness New York Regional Research Center Grant (C-NY05-0705-0312), the Joel Hoffman Fund, Charles Culpeper Scholarship, Irma T. Hirschl Charitable Trust, and Gebroe Family Foundation. K.J.W. is supported by the National Institute of Health (5T32EY013933, 5T32DK00 7647-20). V.B.M. is supported by the National Institute of Health (KJ.M.S. is supported by the National Institute of

Health 08EY020530) and Research to Prevent Blindness, New York, NY, USA. J.M.S. is supported by the National Institute of Health (1F32EY022280-01A1).

REFERENCES

1. Pastor, J.C., de la Rua, E.R. and Martin, F. (2002) Proliferative vitreoretinopathy: risk factors and pathobiology. *Prog. Retin. Eye Res.*, **21**, 127–144.
2. Frank, R.N. (2004) Diabetic retinopathy. *N. Engl. J. Med.*, **350**, 48–58.
3. Caspi, R.R. (2010) A look at autoimmunity and inflammation in the eye. *J. Clin. Invest.*, **120**, 3073–3083.
4. Mahajan, V.B., Skeie, J.M., Bassuk, A.G., Fingert, J.H., Braun, T.A., Daggett, H.T., Folk, J.C., Sheffield, V.C. and Stone, E.M. (2012) Calpain-5 mutations cause autoimmune uveitis, retinal neovascularization, and photoreceptor degeneration. *PLoS Genet.*, **8**, e1003001.
5. Syntichaki, P., Xu, K., Driscoll, M. and Tavernarakis, N. (2002) Specific aspartyl and calpain proteases are required for neurodegeneration in *C. elegans*. *Nature*, **419**, 939–944.
6. Zatz, M. and Starling, A. (2005) Calpains and disease. *N. Engl. J. Med.*, **352**, 2413–2423.
7. Campbell, R.L. and Davies, P.L. (2012) Structure-function relationships in calpains. *Biochem. J.*, **447**, 335–351.
8. Polster, B.M., Basanez, G., Etxebarria, A., Hardwick, J.M. and Nicholls, D.G. (2005) Calpain I induces cleavage and release of apoptosis-inducing factor from isolated mitochondria. *J. Biol. Chem.*, **280**, 6447–6454.
9. Tlucek, P.S., Folk, J.C., Orien, J.A., Stone, E.M. and Mahajan, V.B. (2012) Inhibition of neovascularization but not fibrosis with the fluocinolone acetonide implant in autosomal dominant neovascular inflammatory vitreoretinopathy. *Arch. Ophthalmol.*, **130**, 1395–1401.
10. Tlucek, P.S., Folk, J.C., Sobol, W.M. and Mahajan, V.B. (2013) Surgical management of fibrotic encapsulation of the fluocinolone acetonide implant in CAPN5-associated proliferative vitreoretinopathy. *Clin. Ophthalmol.*, **7**, 1093–1098.
11. Bennett, S.R., Folk, J.C., Kimura, A.E., Russell, S.R., Stone, E.M. and Raphtis, E.M. (1990) Autosomal dominant neovascular inflammatory vitreoretinopathy. *Ophthalmology*, **97**, 1125–1135; discussion 1135–1126.
12. Davis, R.J., Tosi, J., Janisch, K.M., Kasanuki, J.M., Wang, N.K., Kong, J., Tsui, I., Cilluffo, M., Woodruff, M.L., Fain, G.L. *et al.* (2008) Functional rescue of degenerating photoreceptors in mice homozygous for a hypomorphic cGMP phosphodiesterase 6 b allele (Pde6bH620Q). *Invest. Ophthalmol. Vis. Sci.*, **49**, 5067–5076.
13. Tosi, J., Sancho-Pelluz, J., Davis, R.J., Hsu, C.W., Wolpert, K.V., Sengillo, J.D., Lin, C.S. and Tsang, S.H. (2011) Lentivirus-mediated expression of cDNA and shRNA slows degeneration in retinitis pigmentosa. *Exp. Biol. Med.*, **236**, 1211–1217.
14. Neumar, R.W., Xu, Y.A., Gada, H., Guttmann, R.P. and Siman, R. (2003) Cross-talk between calpain and caspase proteolytic systems during neuronal apoptosis. *J. Biol. Chem.*, **278**, 14162–14167.
15. Feng, Z.H., Hao, J., Ye, L., Dayao, C., Yan, N., Yan, Y., Chu, L. and Shi, F.D. (2011) Overexpression of μ-calpain in the anterior temporal neocortex of patients with intractable epilepsy correlates with clinicopathological characteristics. *Seizure*, **20**, 395–401.
16. Lakshmikuttyamma, A., Selvakumar, P., Kanthan, R., Kanthan, S.C. and Sharma, R.K. (2004) Overexpression of m-calpain in human colorectal adenocarcinomas. *Cancer Epidemiol. Biomarkers Prev.*, **13**, 1604–1609.
17. Storr, S.J., Carragher, N.O., Frame, M.C., Parr, T. and Martin, S.G. (2011) The calpain system and cancer. *Nat. Rev. Cancer*, **11**, 364–374.
18. Wert, K.J., Davis, R.J., Sancho-Pelluz, J., Nishina, P.M. and Tsang, S.H. (2013) Gene therapy provides long-term visual function in a pre-clinical model of retinitis pigmentosa. *Hum. Mol. Genet.*, **22**, 558–567.
19. Mahajan, V.B., Vallone, J.G., Lin, J.H., Mullins, R.F., Ko, A.C., Folk, J.C. and Stone, E.M. (2010) T-cell infiltration in autosomal dominant neovascular inflammatory vitreoretinopathy. *Mol. Vis.*, **16**, 1034–1040.
20. Mahajan, V.B. and Lin, J.H. (2013) Lymphocyte Infiltration in CAPN5 autosomal dominant neovascular inflammatory vitreoretinopathy. *Clin. Ophthalmol.*, **7**, 1339–1345.
21. Burkard, N., Becher, J., Heindl, C., Neyses, L., Schuh, K. and Ritter, O. (2005) Targeted proteolysis sustains calcineurin activation. *Circulation*, **111**, 1045–1053.
22. Curcio, C.A., Owsley, C. and Jackson, G.R. (2000) Spare the rods, save the cones in aging and age-related maculopathy. *Invest. Ophthalmol. Vis. Sci.*, **41**, 2015–2018.
23. Jackson, G.R., Owsley, C. and Curcio, C.A. (2002) Photoreceptor degeneration and dysfunction in aging and age-related maculopathy. *Ageing Res. Rev.*, **1**, 381–396.
24. Koh, A.H., Hogg, C.R. and Holder, G.E. (2001) The incidence of negative ERG in clinical practice. *Doc. Ophthalmol.*, **102**, 19–30.
25. Forrester, J.V., Klaska, I.P., Yu, T. and Kuffova, L. (2013) Uveitis in mouse and man. *Int. Rev. Immunol.*, **32**, 76–96.
26. Yadav, U.C. and Ramana, K.V. (2013) Endotoxin-induced uveitis in rodents. *Methods Mol. Biol.*, **1031**, 155–162.
27. Wert, K.J., Skeie, J.M., Davis, R.J., Tsang, S.H. and Mahajan, V.B. (2012) Subretinal injection of gene therapy vectors and stem cells in the perinatal mouse eye. *J. Visual. Exp.*, (69), e4286.
28. Imai, S., Shimazawa, M., Nakanishi, T., Tsuruma, K. and Hara, H. (2010) Calpain inhibitor protects cells against light-induced retinal degeneration. *J. Pharmacol. Exp. Ther.*, **335**, 645–652.
29. David, J., Melamud, A., Kesner, L., Roth, S., Rosenbaum, P.S., Barone, F.C., Popp, S., Hassen, G.W., Stracher, A. and Rosenbaum, D.M. (2011) A novel calpain inhibitor for treatment of transient retinal ischemia in the rat. *Neuroreport*, **22**, 633–636.
30. Nguyen, A.T., Campbell, M., Kenna, P.F., Kiang, A.S., Tam, L., Humphries, M.M. and Humphries, P. (2012) Calpain and photoreceptor apoptosis. *Adv. Exp. Med. Biol.*, **723**, 547–552.
31. Ozaki, T., Nakazawa, M., Yamashita, T., Sorimachi, H., Hata, S., Tomita, H., Isago, H., Baba, A. and Ishiguro, S. (2012) Intravitreal injection or topical eye-drop application of a mu-calpain C2L domain peptide protects against photoreceptor cell death in Royal College of Surgeons' rats, a model of retinitis pigmentosa. *Biochim. Biophys. Acta*, **1822**, 1783–1795.
32. Rowell, H.A., Bassuk, A.G. and Mahajan, V.B. (2012) Monozygotic twins with CAPN5 autosomal dominant neovascular inflammatory vitreoretinopathy. *Clin. Ophthalmol.*, **6**, 2037–2044.
33. Wert, K.J., Sancho-Pelluz, J. and Tsang, S.H. (2014) Mid-stage intervention achieves similar efficacy as conventional early-stage treatment using gene therapy in a pre-clinical model of retinitis pigmentosa. *Hum. Mol. Genet.*, **23**, 514–523.
34. Hood, D.C. and Birch, D.G. (1992) A computational model of the amplitude and implicit time of the b-wave of the human ERG. *Vis. Neurosci.*, **8**, 107–126.
35. Hood, D.C. and Birch, D.G. (1994) Rod phototransduction in retinitis pigmentosa: estimation and interpretation of parameters derived from the rod a-wave. *Invest. Ophthalmol. Vis. Sci.*, **35**, 2948–2961.
36. Tsang, S.H., Burns, M.E., Calvert, P.D., Gouras, P., Baylor, D.A., Goff, S.P. and Arshavsky, V.Y. (1998) Role for the target enzyme in deactivation of photoreceptor G protein in vivo. *Science*, **282**, 117–121.
37. Skeie, J.M., Tsang, S.H. and Mahajan, V.B. (2011) Evisceration of mouse vitreous and retina for proteomic analyses. *J. Visual. Exp.*, (50), e2795.